Proc. Natl. Acad. Sci. USA
Vol. 86, pp. 6143–6147, August 1989
Biophysics

In-plane phase transition of an integral membrane protein: Nucleation of the OmpF matrix porin rectangular polymorph

(electron diffraction/electron microscopy/diffuse scattering/image processing/rotational disorder)

DOUGLAS L. DORSET*, ANDREW K. MASSALSKI*, AND JÜRG P. ROSENBUSCH†

*Electron Diffraction Department, Medical Foundation of Buffalo, Inc., 73 High Street, Buffalo, NY 14203; and †Abteilung Mikrobiologie, Biozentrum der Universität Basel, Klingelbergstrasse 70, CH-4056 Basel, Switzerland

Communicated by David Harker, May 30, 1989 (received for review January 25, 1989)

ABSTRACT **A hexagonal polymorph (a = 79 Å) of OmpF matrix porin from *Escherichia coli* spontaneously transforms to a rectangular form (a = 79 Å, b = 137 Å) after several months' storage in the refrigerator. Nucleation of this second polymorph is first disclosed by diffuse streaks in electron diffraction patterns or in computer-generated Fourier transforms of electron microscope images. With time, this streaking is resolved as an apparent superlattice, and eventually domains of orthorhombic polymorph are detected in the parent hexagonal lattice that can be oriented in either of three directions, depending on the polarity of the orthorhombic crystal growth. Models for this phenomenon based on protein trimer rotation successfully explain the progress of the phase transition and, if protein–protein interactions are the most important interactions between adjacent trimers in the lipid matrix, the transition is quite similar to what occurs with molecular crystals.**

Three genetically related transmembrane channel-forming proteins from the outer membrane of *Escherichia coli*—i.e., the so-called "porins" (OmpF, OmpC, or PhoE)—have been studied extensively by electron microscopy (1–6) in order to determine their functional behavior as molecular sieves for water-soluble materials that can be transported into the bacterial periplasm (7–9). Initial two-dimensional studies with negatively stained preparations either *in situ* (1) or in reconstituted vesicle crystals (2, 4–6) revealed that these porins are associated as trimers with three strain-accumulating regions tentatively identified as the channel openings. The pore geometry in the OmpF porin was later revealed in three-dimensional tomographic reconstructions made from electron micrographs taken at various tilts around several axes through the unit cell (3), and the existence of a transmembrane channel was demonstrated at *ca.* 20 Å resolution. Subsequent high-resolution (e.g., 8.5 Å) studies on a cryomicroscope with preparations embedded in various media (10, 11) began to locate regions of the protein trimer that might be the predominately β-sheet polypeptide secondary structure indicated by spectroscopic (12, 13) and x-ray diffraction studies (13). More recently, detail has been observed to 3.2 Å resolution (H. J. Sass, A.K.M., and F. Zemlin, unpublished data). Similar structural features have been found in recent high-resolution studies of the PhoE porin (6).

Depending on the conditions used for reconstitution, at least three different planar crystal polymorphs have been found for OmpF porin (2). At high phospholipid-to-protein ratios, a hexagonal form is found with lattice dimensions (plane group p3, a = 93 Å) similar to a three-dimensional crystal hexagonal form used for x-ray crystallographic studies (14). This can be treated with phospholipase A_2 (15) to produce a significantly contracted hexagonal lattice (a = 72 Å), which has permitted the highest resolution studies cited above. When allowed to age for several months, the larger hexagonal form is also found to lose lipid spontaneously to form a smaller hexagonal polymorph (a = 79 Å) that can coexist with a rectangular form (plane group pmg, a = 79 Å, b = 137 Å). These forms can also be formed by reconstitution with a lower lipid-to-protein ratio. At 20 Å resolution, three-dimensional images (3) indicate that the underlying porin trimer structure is the same for all three forms.

In the initial structural work, the rectangular form was only rarely encountered in lipid porin preparations. More recently, it has been found that a slow phase transition, involving a trimer rotation around the threefold axis, takes place from the small hexagonal to rectangular polymorph to eventually produce samples that are relatively rich in the rectangular form. As shown in this paper, the initial stage of this transition is detected by the presence of directional streaks in diffraction patterns from the hexagonal form that slowly acquire the features of a threefold disordered orthorhombic diffraction pattern.

MATERIALS AND METHODS

Two-Dimensional Porin Crystals. As described earlier in detail (16), optimal conditions for reconstitution of OmpF matrix porin as two dimensionally crystalline vesicles in 1,2-dimyristoyl-*sn*-glycerophosphocholine was achieved after numerous systematic changes of relevant variables. Various lipid-to-protein ratios were used and the more compact unit cells were achieved when lipid-to-protein ratios = 0.16. Prior to electron microscopic study, the flattened vesicles (diameter ≥ 10 μm), which have been observed to form ordered double membrane stacks (3), were negatively stained with 2% uranyl acetate after the specimen was first washed with Tris·HCl buffer.

Electron Microscopy and Diffraction. Electron microscopy and diffraction experiments on the negatively stained vesicle sheets were carried out on a JEOL JEM-100B electron microscope operated at 100 kV. Images were photographed on either DuPont Cronex or Kodak DEF-5 film at a direct magnification of ×20,000. High-dispersion electron diffraction patterns were photographed on Kodak DEF-5 film using the condenser lens system to isolate a <1-μm diameter region of the specimen (17).

Image Evaluation and Analysis. The crystallinity of individual vesicle sheets was initially evaluated by scanning laser-illuminated electron microscope images on an optical bench, thus allowing one to observe the resolution of optical diffraction patterns. After suitable areas were identified, they were scanned at 25-μm raster with an Optronics P1000 rotating drum densitometer to produce a digitized image file in a VAX 8600 computer, which could be manipulated by using the IMAGIC image processing software (18). Typical procedures included Fourier-peak-filtration, in which a mask is placed over the computed image transform to band-pass only the Bragg spots in the reverse Fourier transform. This produces an average image, which is presumably free of

The publication costs of this article were defrayed in part by page charge payment. This article must therefore be hereby marked "*advertisement*" in accordance with 18 U.S.C. §1734 solely to indicate this fact.

continuous noise perturbations that may arise from uneven stain distribution, radiation damage, etc. (19). Another image averaging technique employed in this study is cross-correlation in real space, where a small Fourier-peak-filtered image is compared to the experimental image to find areas of maximal overlap so that an average of subregions in the crystallographically most perfect regions of the specimen can be accumulated in image space. This cross-correlation function, represented by

$$\phi(h'k') = \frac{1}{N}\sum_h \sum_k F(hk)G(h + h', k + k')$$

(20), will produce maxima during shifting when F and G overlap. As will be seen, this latter technique can also be used to compare phase-transformed crystalline domains within a larger crystalline area having a different average symmetry. In our experimental work on negatively stained preparations the difference between hexagonal and orthorhombic arrays is easily distinguished by this technique, when appropriate thresholds are imposed.

Model Calculations. As in earlier simulations of n-beam dynamical scattering from negatively stained membrane proteins (21), a density model for OmpF porin was constructed initially by including uranium sites within the projected circular confines of the pore and imposing a rather large temperature factor to each uranium atom. This leads to an unnecessarily large-scale structure factor calculation, particularly if non-integral Miller indices are computed to produce the continuous transform of a unit cell. The model can be scaled down by reducing the unit cell axes 10-fold and then placing single uranium atoms on a correspondingly reduced trimer model to simulate each pore site. The approximate Gaussian fall-off of the scattering factor, f_u, is broadened by an isotropic temperature factor with $B = 20$ Å^2. This simulates the stain density at each pore on a miniaturized scale, requiring only one atom coordinate for a single pore location

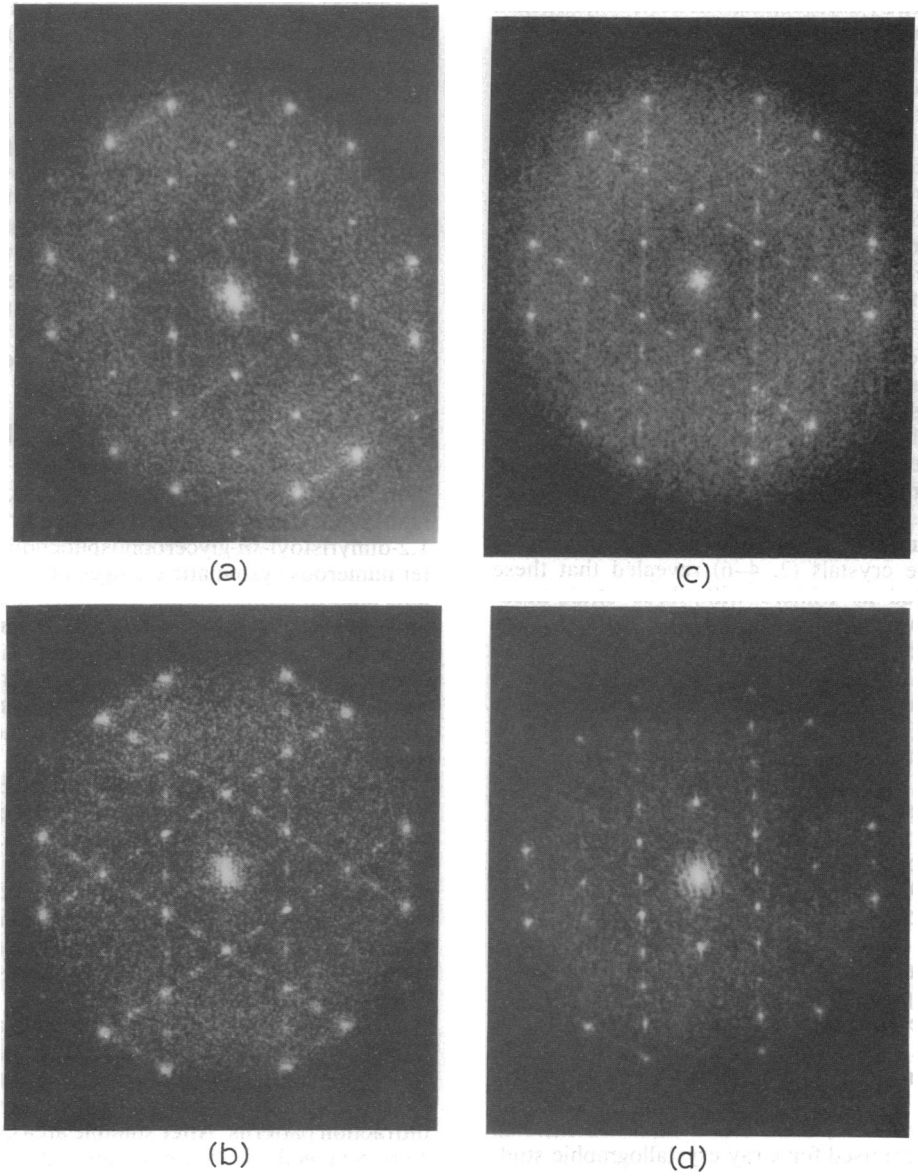

FIG. 1. As shown in an earlier report (23), the existence of a phase transition in OmpF crystals is indicated in the earliest stages by continuous diffuse scatter around {110} reflections, but the Bragg reflections still represent an overall hexagonal symmetry. Further stages of the phase transformation result in the appearance of a superlattice pattern. (*a*) Initially, the Bragg pattern is still that of the perfect hexagonal packing but strongest diffuse streaks now link {100} spots. (*b*) Later, the streaks are resolved as Bragg spots corresponding to a threefold disordered orthorhombic unit cell. The existence of the orthorhombic unit cell is evident when smaller image areas are Fourier-transformed (*c* and *d*) to demonstrate the existence of single crystal subdomains with different polarities. Two orthorhombic orientations are found in the sampled area in *c*, whereas only one orientation exists in *d*.

in a disordered lattice. (The validity of this approximation is verified by a near-match of computed diffraction intensities to the previous model. Again, it should be stressed that the uranium scattering factor modulated by a Debye–Waller factor is only used here for its near-Gaussian property and for ease of computation. Any Gaussian model with proper dimensions would be appropriate here.)

Model structure factor calculations were carried out in the usual way—i.e.,

$$F(\mathbf{s}) = \sum f'_u \exp 2\pi i(\mathbf{r}\cdot\mathbf{s}),$$

where $f'_u = f_u \exp(-B\sin^2\theta/\lambda^2)$. The calculation is either made with integral or non-integral Miller indices. Initial models of continuous scattering utilized the Laue equation (22) in which the diffuse scattering from a disordered structure is expressed by

$$I(\mathbf{s}) = c_A c_B (f_A - f_B)^2 \left(1 + 2\sum \alpha_m \cos 2\pi \mathbf{s}\cdot\mathbf{x}_m\right). \quad [1]$$

The scattering factors for trimer arrays A and B, respectively, from disordered and perfectly ordered structures are compared such that correlations along vectors x_m can also be considered. This model structure is like an alloy in which a trimer "atom" can be randomly or systematically replaced by a rotated trimer "impurity." Later calculations were based on the superlattice structure model described below.

RESULTS AND ANALYSIS

As shown in a preliminary report (23), the very initial stages of a phase transition in the a = 79 Å hexagonal crystal structure of OmpF porin are evidenced by the directional diffuse scattering around the {110} reflections seen both in hexagonal electron diffraction patterns and in computed Fourier transforms of large image areas. A comparison of continuous diffraction from a perfect hexagonal lattice to that from a packing deformed by disorder of the first kind (22)—i.e., a quasi-temperature factor—places diffuse scatter around the {110} reflections but also components near the central beam that are not seen experimentally. Use of the Laue equation (Eq. 1) was more successful when the hexagonal lattice is compared to one with trimers randomly rotated by 60°. In the latter model, the diffuse scatter is now located near the {110} reflections only, and it is more intense than in the previous calculation of quasi-thermal disorder.

After some time has elapsed, the streaked pattern eventually transforms to an apparent orthorhombic superlattice with dimensions a = 284.0 Å, b = 164.0 Å. First, one notes an array of streaks in locations different from those seen initially (23) (Fig. 1*a*). After the preparation is allowed to stand for a long enough period, the superlattice spots appear as seen in Fig. 1*b*, *if the image of a large enough specimen area is Fourier-transformed to its diffraction pattern.* Smaller image areas, however, are transformed to other diffraction motifs (Fig. 1 *c* and *d*), which reveal that the superlattice pattern in Fig. 1*b* is actually a superposition of three orthorhombic diffraction patterns mutually rotated by 120°.

If the superlattice indicated by the diffraction pattern in Fig. 1*b* is a perfect hexagonal packing array (Fig. 2*a*), then its computed transform will, of course, be no different from that of a single unit cell with plane group symmetry p3 (Fig. 2*b*). Rotation of one trimer in Fig. 2*a* by 60° (Fig. 2*c*) breaks the hexagonal symmetry and results in diffuse scattering concentrated near the {110} reflections (Fig. 2*d*), in agreement with the model diffraction pattern illustrated in our preliminary study (23). Rotation of two trimers as in Fig. 2*e* to nucleate an orthorhombic subdomain causes the intensity of the superlattice spots to be concentrated in bands corresponding to the polar direction of the orthorhombic cell (Fig. 2*f*). These bands will be narrowed as more molecules contribute to the orthorhombic nucleus (Fig. 2*g* transforms to Fig. 2*h*), until a

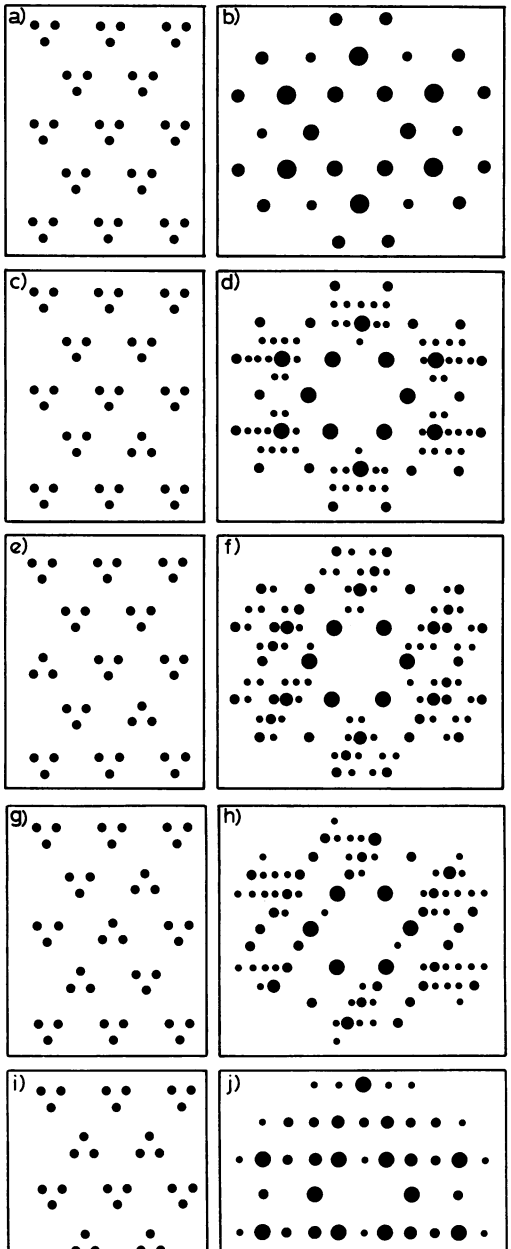

FIG. 2. Explanation of the phase transformation based on a superlattice with dimensions suggested by the Fourier transform in Fig. 1*b*. (*a*) Perfect hexagonal packing of porin trimers. Its Fourier transform (*b*) is found in studies of freshly prepared porin crystal sheets. (*c*) If one trimer is rotated around its threefold axis by 60°, the Bragg intensities of the Fourier transform are near those of a perfect hexagonal array (*d*), but diffuse intensity occurs around the {110} reflections. This matches the calculations of rotational disorder based on use of the Laue equation (Eq. 1) in our preliminary study (23). (*e*) Two trimers rotated by 60° can form the nucleus of an orthorhombic crystal. Its Fourier transform (*f*) contains diffuse bands that now intersect {100} and {110} reflections of the hexagonal Bragg pattern. The orthorhombic nucleus can grow to three rotated trimers (*g*), for which the diffuse diffracted intensity becomes more intense and concentrated to narrower bands (*h*). Finally, the orthorhombic structure is reached (*i*) with a characteristic Fourier transform (*j*). A threefold rotation of this pattern will reproduce the pattern in Fig. 1*b* just as a threefold rotation of *f* will reproduce Fig. 1*a*.

large enough area is transformed to minimize the shape envelope broadening of the orthorhombic cell (Fig. 2*i* transforms to Fig. 2*j*). The new orthorhombic cell, however, can be nucleated in any of three possible directions in the original hexagonal lattice so that domains of orthorhombic polymorph can be rotated away from other areas by $n \cdot 120°$; this produces the diffraction pattern in Fig. 1*b*, when enough of the partially phase-transformed crystal is included in the Fourier transform. Implicit also in this process is the creation of twin boundaries when all of the two-dimensional crystal patch has converted to the orthorhombic structure.

One can see from the above that the concentration of diffuse scattering around {110} reflections found in the beginning of the transition (23) is the consequence of a random distribution of trimers that are rotated by 60° within the predominately hexagonal lattice. Elongation of these bands appears to be due to the formation of larger orthorhombic nuclei within the predominately hexagonal structure.

Evidence for the rotationally oriented orthorhombic domains also can be found directly in real space by cross-correlation techniques. If, for example, a crystalline patch has a Fourier transform apparently made up of two superimposed orthorhombic patterns (Fig. 1*c*), the area corresponding to one of them can be isolated and an average orthorhombic packing can be produced by reverse transformation via peak filtration (Fig. 3*a*). Its location in the overall image can be verified by cross-correlation techniques as the only region in which the motif of cross-correlation peaks corresponds to the sample space lattice repeat (Fig. 3*b*). Rotation of the sample orthorhombic lattice by 120° will locate the other domain in another cross-correlation map in the predominately hexagonal structure (Fig. 3*d*) in which yet another orthorhombic packing has been nucleated along a second orientation (Fig. 3*c*).

DISCUSSION

From the observations presented above, it is first of all apparent that diffuse scattering in electron diffraction patterns or computed Fourier transforms from reconstituted membrane protein crystals must be scrutinized carefully,

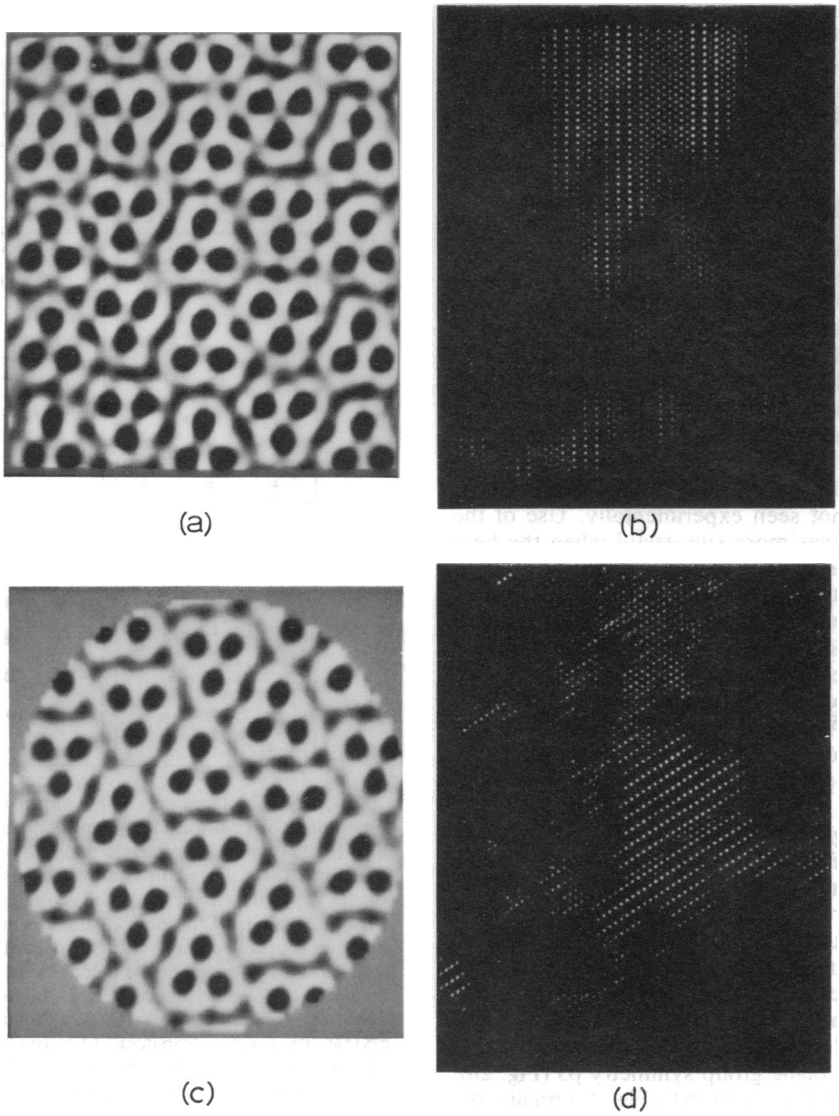

FIG. 3. Experimental demonstration of the rotationally disordered orthorhombic subdomain by a cross-correlation technique. A computed Fourier transform of an experimental electron microscope image shown in Fig. 1*c* was found with only two sets of superlattice lines through hexagonal {100} reflections, oriented 60° from one another. By choosing a small enough image area, one domain can be found with perfect orthorhombic packing and its structure visualized (*a*) by Fourier peak filtration. By using an average structure based on this filtration, the area of the total image with this orientation can be found by the location of intense cross-correlation peaks (*b*). By rotating the reference image (*a*) by 120° the second, smaller subdomain in the image can be found by a cross-correlation map (*d*) and the peak-filtered image (*c*) of this subarea (obtained by a reverse Fourier-transform) can be used to verify its presence as an orthorhombic packing rotated away from the other subarea.

because it might not be merely experimental noise. The presence of directional diffuse scattering in diffraction patterns from—e.g., molecular crystals—has been often used advantageously to analyze packing disorders due to defect incorporation (24), reorientation of subgroups (25), statistical variations in occupancy or molecular orientation (26), in addition to analysis of thermal motion (27). Recently, such analysis has also been employed in protein x-ray crystallography to detect correlated or uncorrelated molecular motions within the crystal (28–30). The use of non-Bragg scattering reported in this paper is more analogous to the analysis of solid solution alloy structures (22). In the case described, diffuse scattering is the first indication of a phase transition in reconstituted OmpF matrix porin crystals, demonstrating that the protein trimers have the possibility for in-plane rotation, even when there is a small amount of lipid.

The reason for the hexagonal-to-orthorhombic transition in this membrane protein is not entirely clear because the nature of protein–protein and protein–lipid interactions is not yet understood for these reconstituted crystalline sheets. Some clues might be found in recent analyses of the forces responsible for the intraplanar interaction of other membrane proteins (31–36). It is shown that protein–lipid interactions must be much less important than protein–protein interactions in some cases in order to control the aggregation geometry of these integral membrane proteins. In other cases, lipid mediation is important (34). The types of protein–protein interactions might include pure volume exclusion, either in terms of hard disk (31, 33) or soft disc (31, 33, 36) models. Additionally, evidence can be found for particle–particle electrostatic repulsions (33, 35) or attractions (33) in addition to the steric interactions between disks. Such interactions for the OmpF porin would lead to strong repulsions at close interprotein contacts resulting in packing constraints similar to those found in small molecules (37).

We may speculate that the progress of the phase transition, therefore, might be understood in terms of symmetry change. The hexagonal packing motif in Fig. 2*a* has fewer molecular contacts than the orthorhombic form (Fig. 2*i*) and is therefore metastable. A 60° rotation of the porin trimer is enough to optimize protein–protein contacts to produce the lower energy orthorhombic packing. That this nucleation is a process requiring several months indicates that the activation energy for this rotation is somewhat large. On the other hand, an orthorhombic lattice apparently is not produced directly from the larger hexagonal form, which contains more phospholipid. In this case, lipid in interprotein regions effectively modulates the repulsive forces between protein trimers assumed in our model. The lesser importance of protein–protein interactions for the larger hexagonal form may also explain the paracrystalline lattice distortion found for this lipid-rich two-dimensional crystal form.

We thank Dr. Robert Blessing for a critical review of the manuscript. Research described in this paper was funded by a grant from the National Institutes of Health (GM21047).

1. Steven, A. C., ten Heggler, B., Müller, R., Kistler, J. & Rosenbusch, J. P. (1977) *J. Cell Biol.* **72,** 292–301.
2. Dorset, D. L., Engel, A., Häner, M., Massalski, A. & Rosenbusch, J. P. (1983) *J. Mol. Biol.* **165,** 701–710.
3. Engel, A., Massalski, A., Schindler, H., Dorset, D. L. & Rosenbusch, J. P. (1985) *Nature (London)* **317,** 643–645.
4. Chang, C.-F., Mizushima, S. & Glaeser, R. M. (1985) *Biophys. J.* **47,** 629–639.
5. Jap, B. K. (1988) *J. Mol. Biol.* **199,** 229–231.
6. Jap, B. K. (1989) *J. Mol. Biol.* **205,** 407–419.
7. Nikaido, H. & Rosenberg, E. Y. (1981) *J. Gen. Physiol.* **77,** 121–135.
8. Schindler, H. & Rosenbusch, J. P. (1978) *Proc. Natl. Acad. Sci. USA* **75,** 3751–3755.
9. Schindler, H. & Rosenbusch, J. P. (1981) *Proc. Natl. Acad. Sci. USA* **78,** 2302–2306.
10. Massalski, A., Sass, H. J., Zemlin, F., Beckmann, E., van Heel, M., Büldt, G., Dorset, D. L., Zeitler, E. & Rosenbusch, J. P. (1987) in *Proceedings of the Electron Microscopy Society of America, 45th Annual Meeting, Baltimore, Maryland,* ed. Bailey, G. W. (San Francisco Press, San Francisco), pp. 788–789.
11. Sass, H. J., Massalski, A., Zemlin, F., Beckmann, E., van Heel, M., Büldt, G., Dorset, D. L., Zeitler, E. & Rosenbusch, J. P. (1987) in *Proceedings of the Electron Microscopy Society of America, 45th Annual Meeting, Baltimore, Maryland,* ed. Bailey, G. W. (San Francisco Press, San Francisco), pp. 790–791.
12. Rosenbusch, J. P. (1974) *J. Biol. Chem.* **249,** 8019–8029.
13. Kleffel, B., Garavito, R. M., Baumeister, W. & Rosenbusch, J. P. (1985) *EMBO J.* **4,** 1589–1592.
14. Garavito, R. M., Jenkins, J., Jansonius, J. N., Karlson, R. & Rosenbusch, J. P. (1983) *J. Mol. Biol.* **164,** 313–327.
15. Mannella, C. A. (1984) *Science* **224,** 165–166.
16. Rosenbusch, J. P., Garavito, R. M., Dorset, D. L. & Engel, A. (1981) in *Protides of the Biological Fluids,* ed. Peeters, H. (Pergamon, Oxford), pp. 171–174.
17. Ferrier, R. P. (1969) *Adv. Opt. Electron Microsc.* **3,** 155–218.
18. van Heel, M. & Keegstra, W. (1981) *Ultramicroscopy* **7,** 113–130.
19. Misell, D. L. (1978) *Image Analysis, Enhancement and Interpretation* (North-Holland, Amsterdam), pp. 142–147.
20. Frank, J. (1980) in *Computer Processing of Electron Microscope Images,* ed. Hawkes, P. W. (Springer, Berlin), pp. 187–222.
21. Dorset, D. L. (1984) *Ultramicroscopy* **13,** 311–324.
22. Guinier, A. (1963) *X-Ray Diffraction in Crystals, Imperfect Crystals, and Amorphous Bodies* (Freeman, San Francisco), pp. 262–267.
23. Dorset, D. L. & Massalski, A. (1986) in *Proceedings of the Electron Microscopy Society of America, 44th Annual Meeting, Albuquerque, New Mexico,* ed. Bailey, G. W. (San Francisco Press, San Francisco), pp. 166–167.
24. Glover, D. M. (1987) *Acta Crystallogr. Sect. A* **37,** 251–263.
25. Hoppe, W. (1957) *Z. Kristallogr. Kristallgeom. Kristallphys. Kristallchem.* **108,** 335–340.
26. Epstein, J., Welberry, T. R. & Jones, R. D. G. (1982) *Acta Crystallogr. Sect. A* **38,** 611–618.
27. Hoppe, W. (1956) *Z. Kristallogr. Kristallgeom. Kristallphys. Kristallchem.* **107,** 406–432.
28. Phillips, G. N., Jr., Fillers, J. P. & Cohen, C. (1980) *Biophys. J.* **32,** 485–502.
29. Doucet, J. & Benoit, J. P. (1987) *Nature (London)* **325,** 643–646.
30. Caspar, D. L. D., Clarage, J., Salunke, D. M. & Clarage, M. (1988) *Nature (London)* **332,** 659–662.
31. Markovics, J., Glass, L. & Maul, G. G. (1974) *Exp. Cell Res.* **85,** 443–451.
32. Pearson, R. H., Hui, S. W. & Stewart, T. P. (1979) *Biochim. Biophys. Acta* **557,** 265–282.
33. Pearson, L. T., Chan, S. I., Lewis, B. A. & Engelman, D. M. (1983) *Biophys. J.* **43,** 167–174.
34. Pearson, L. T., Edelman, J. & Chan, S. I. (1984) *Biophys. J.* **45,** 863–871.
35. Abney, J. R., Braun, J. & Owicki, J. C. (1987) *Biophys. J.* **52,** 441–454.
36. Braun, J., Abney, J. R. & Owicki, J. C. (1987) *Biophys. J.* **52,** 427–439.
37. Kitaigorodskii, A. I. (1961) *Organic Chemical Crystallography* (Consultants Bureau, New York).